

Carrier capture efficiency and amplification properties of asymmetrical multiple quantum well optical amplifiers

V. V. LYSAK^{a,b*}, I. A. SUKHOIVANOV^c, YONG TAK LEE^a

^a*Department of information and communication, Gwangju Institute of science and technology (GIST), 1 Oryong-dong, Buk-ku, Gwangju, 500-712, Republic of Korea*

^b*Laboratory "Photonics", Kharkov National University of Radio Electronics, 14, Lenin av., Kharkov, 61166, Ukraine*

^c*Departamento de Electronica, FIMEE, Guanajuato University, P.O. Box 215-A, Salamanca, GTO, 36730, Mexico*

A numerical model for calculating the carrier transport properties in asymmetrical multiple quantum-well (AMQW) structures is extended with more exact calculation of carrier-dependent capture efficiency for each QW including internal optical field in the whole structure. Using this extended model, the amplification spectra of an asymmetrical 6-QW SOA are calculated. The simulation results show excellent agreement with experimental data over the whole range of carrier injection and for a wavelength range of more than 160 nm.

(Received February 15, 2006; accepted March 23, 2006)

Keywords: Asymmetrical multiple quantum-well semiconductor optical amplifier, Carrier transport, Modeling

1. Introduction

Semiconductor optical amplifiers (SOAs) are optoelectronic devices offering promising features for the optical treatment of information. This technology has a particular advantage of being capable of performing multiple operations simultaneously, such as wavelength conversion and all-optical demultiplexing, as well as providing linear gain.

Although many different SOA structures have been proposed, in all cases the active region consists of bulk [1], multiple quantum wells (MQWs) [2], quantum dots materials [3], or asymmetrical MQW (AMQW) structures. In AMQW structures active region consists of MQWs of varying thickness and/or composition [4]. If designed properly, AMQW SOAs have the potential to provide a spectral gain range more than twice as broad as in conventional MQW SOAs [5]. This is achieved due to each QW or the group of identical QWs provides optical gain in the definite wavelength range. As a result the very wide gain spectrum becomes possible, which allows amplification of ultra-short pulses. However, combination of different QWs in a single active region influences greatly the carrier transport processes, which in turns affect the amplification properties of SOA. Earlier we have shown that in AMQW transport processes play the key role and define population dynamics, temperature dynamics, and gain dynamics in each QW composing an AMQW.

One of the approaches for modeling of the gain properties incl. carrier transport effects is the use of a rate-equation model coupled with spectral dependence of the

optical gain and traveling-wave equations for the optical field in the active medium. This approach allows rather quick and efficient modeling, and it has been widely used to describe the transport effects and recombination processes in single QW lasers [6] and conventional MQW lasers [7], as well as the steady-state and dynamic characteristics of MQW [8] and asymmetric dual QW lasers [9]. We use more complex models based on self-consistent solution of the Maxwell-Bloch, Schrödinger, drift-diffusion and Poisson equations for more detailed modeling of transport effects in the complex AMQW active medium than it allows rate equations approach [10]. Here we will show that tacking into account the carrier-dependent capture under treatment of carrier transport allows better explanation of experimental gain spectra.

The carrier-dependent capture leads to more uniform pumping of the complex AMQW structure resulting in enhancement of the optical gain on shorter wavelengths at larger pumping currents and to best fitting of experimental results.

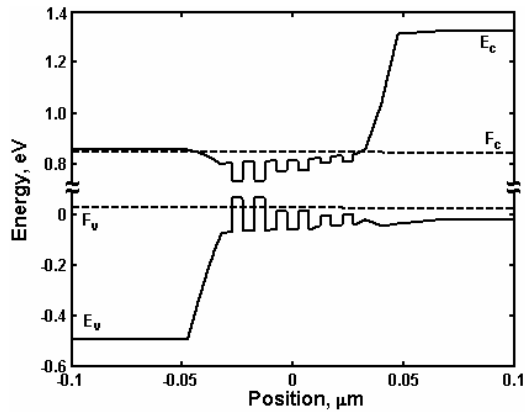
2. Structure description

Here we analyze the structure that consists of 6 $\text{In}_x\text{Ga}_{1-x}\text{As}_y\text{P}_{1-y}$ quantum-well active layers. QWs and barriers have thickness of 5 nm. The transition wavelength for the first two QWs is equal to 1.67 μm , for the middle two QWs is 1.53 μm and for the last two QWs is 1.45 μm . The experiments show that such structure enables a wide 3dB gain bandwidth of up to 100 nm (1.53 μm 1.63 μm) at DC current of 200 mA [11]. It was experimentally clarified that these SOAs can amplify picosecond [12] and sub-picosecond [13] optical pulses and the wavelength

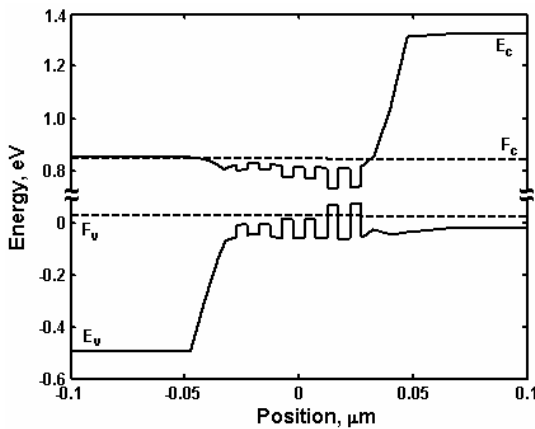
dependence of the gain saturation characteristics is negligible.

3. Band-gap diagram and carrier capture efficiency in AMQW

Previously [11], we have made estimations of static characteristics of this structure using the piecewise constant potential profile of the active region. Here the self-consistent solution of the Schrödinger, drift-diffusion and Poisson equations is used to obtain the band diagram and spatial carrier distribution in AMQW structure. Fig. 1 shows the energy band diagram for the structure with long-wavelength QWs adjacent to a) n-cladding layer and b) p-cladding layer at 120 mA of the pumping current. These results show no change in the quasi-Fermi levels in the active region, but the strong non-uniformity of the potential profile due to high electrical field in the barriers between the shorter wavelength QWs and strong non-uniformity of carrier distribution in different QWs.



a



b

Fig. 1. Calculated band diagram for 6 AMQW SOA with different configurations: longer wavelength QWs are placed at the a) n-cladding layer; b) p-cladding layer.

The spatial distribution of the electron concentration for the structure in Fig. 1a at the different values of pumping current is presented in Fig. 2, showing strong inhomogeneous carrier distribution.

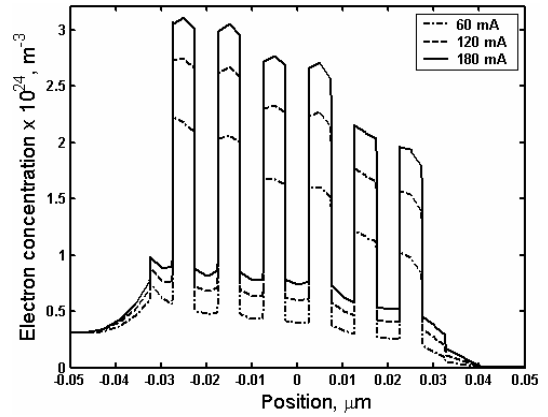


Fig. 2. Electron distribution along the crystal growth axis in structure, which presented in Fig. 1a, at different values of the pumping current.

The gain value depends on the population of bound 2D states in each QW which in turn depends on coupling of the 2D states to unbound 3D states. The simple way to consider this fact is to introduce the capture efficiency, as ratio of 2D carrier concentration N_{2D} in a QW to concentration of 3D carriers N_{3D} in a QW, $\eta_{cap} = N_{2D}/N_{3D}$. It will allow in the frame of rate equations to take account of the carrier spatial distribution inhomogeneity and its influence on the SOA amplification properties.

Assuming common quasi-Fermi level for 2D and 3D carriers in the well region we can express capture efficiency via (local) capture and escape times as:

$$\eta_{xcap} = \frac{\tau_{xesc}}{\tau_{xcap}} = \frac{\int \rho_{x2D}(E) f_x(E, F_x) dE}{\int \rho_{x3D}(E) f_x(E, F_x) dE}, \text{ where } x=e, h,$$

where $\rho_{x2D}(E)$ and $\rho_{x3D}(E)$ are the DOS functions of carriers in the well and capture region, respectively; $f_x(E, F_x)$ is the Fermi factor with F_x is the quasi-Fermi level. Using information about energy levels for electrons and holes, quasi-Fermi levels and density-of-states (DOS) we calculate capture efficiency of carriers (electrons(e) or holes(h)) through (1).

We calculated the dependence on the 2D carrier concentration of capture efficiency in contrast to [7], where authors have used expression (1) to calculate the dependence on total carrier concentration of the emission-to-capture-times ratio. Because we are interested in gain analysis, we investigated only the distribution and interaction of 2D carriers in our model [11]. Fig. 3 shows the electron capture efficiency versus 2D electron concentration for the structure presented in Fig. 1a.

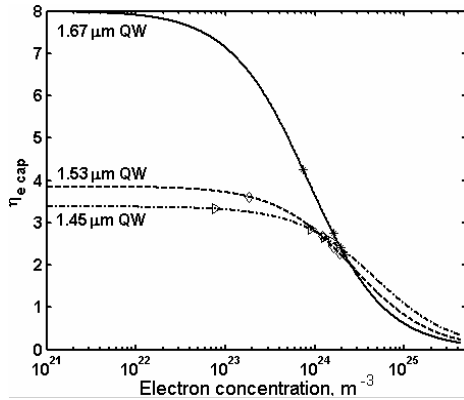


Fig. 3. Dependence of electron-capture efficiency on the electron concentration in each QW inside the AMQW structure presented in Fig. 1a.

Calculated results are presented by stars, diamonds and triangles and fitted results are presented by solid, dashed and dash-dotted lines for 1.67 μm , 1.53 μm and 1.45 μm QW, respectively. At the low values of the 2D carrier concentration the 3D carriers being in the tail of the Fermi distribution. As a result the capture efficiency is almost constant. While 2D carrier concentration increases the quasi-Fermi level shifts towards the unconfined states,

leading to the growth of the occupation probability for the unconfined states. As a consequence the capture efficiency drops rapidly due to the enhanced escape probability. And under concentrations more than about 10^{24} m^{-3} the electron capture efficiency becomes low and nearly equal for all QWs due to saturation of capture process.

The calculated data are fitted by the next expression:

$$\eta_{x\text{cap}} = \eta_{x\text{cap}0} / \left(1 + N / N_{\text{cap},\text{sat}}\right),$$

where is $\eta_{x\text{cap}0}$ is the capture efficiency at the low carrier concentration, N is the 2D carrier concentration and $N_{\text{cap},\text{sat}}$ is the carrier concentration when capture efficiency decreases in two times. In the Table I we compare the capture efficiency of electrons and holes for the presented AMQW structure (Fig. 1a), AMQW structure with inversion position of QWs (Fig. 1b) and for different single quantum well (SQW) structures with material parameters for the transition wavelength 1.67 μm , 1.53 μm and 1.45 μm , respectively. The capture efficiency for holes is larger than for electrons due to larger effective mass.

Table 1. Calculated parameters of capture efficiency for AMQW and different SQW structures.

Parameter		1.67 μm	1.53 μm	1.45 μm
SQW	$\eta_{e\text{cap}0}$	7.96	3.56	3.13
	$N_{\text{cap},\text{sat}}, 10^{24} \text{ m}^{-3}$	0.83	2.35	3.05
	$\eta_{p\text{cap}0}$	37.53	16.2	4.89
	$P_{\text{cap},\text{sat}}, 10^{24} \text{ m}^{-3}$	3.59	15.36	15.79
AMQW	$\eta_{e\text{cap}0}$	7.95	3.87	3.37
	$N_{\text{cap},\text{sat}}, 10^{24} \text{ m}^{-3}$	0.87	2.75	4.89
	$\eta_{p\text{cap}0}$	37.61	16.24	4.98
	$P_{\text{cap},\text{sat}}, 10^{24} \text{ m}^{-3}$	4.07	22.48	24.27
AMQW -inversion	$\eta_{e\text{cap}0}$	7.8	3.86	3.10
	$N_{\text{cap},\text{sat}}, 10^{24} \text{ m}^{-3}$	0.86	2.85	4.61
	$\eta_{p\text{cap}0}$	38.53	16.2	4.99
	$P_{\text{cap},\text{sat}}, 10^{24} \text{ m}^{-3}$	3.76	17.95	18.96

For both electrons and holes the capture efficiency $\eta_{x\text{cap}0}$ is larger for deeper QWs, because of the larger carrier effective mass and DOS. But the parameter $N_{\text{cap},\text{sat}}$ is larger for the shallow QWs, because the electrical field in barriers shifts up the energy band and decreases the difference between the quasi-Fermi level and energy level at high pumping currents and it does not depend on position of such QW in the active layer (see Fig. 1). Since the electrical field in SQW structure is much smaller, the saturation carrier concentration for 1.45 μm QW in the AMQW structure is larger than in SQW, whereas it is almost the same for 1.67 μm QW. The

proposed fitting formula can be easily included into the rate equations providing simple account for carrier inhomogeneity and its influence on the SOA amplification properties.

4. Calculation of the optical gain spectra and comparison with the experiment

The dynamical simulation is based on the time domain model which earlier was applied to investigation of the high-speed properties of QW lasers [7] and MQW SOAs [8], and model for the carrier temperature dynamics in

lasers and QW SOAs [14]. But in our model, the recombination and transport processes in the structure are considered separately for each QW, taking into account the difference in material parameters [15] for each QW and including carrier heating and free carrier absorption for different material parameters and different wavelengths of the input signal [15]. For optical gain calculations we use model derived from semiconductor density matrix equation [16]:

$$G_i(N_{w_i}, N_p, \omega) = \frac{\Gamma_{w_i} v_{g,i} \omega}{\varepsilon_0 \bar{n}} \int_{E_{l,e-h}}^{E_{bar}} \frac{\rho |\mu|^2 (f_c - f_{hh}) \pi L}{1 + N_p / N_{p,s}} dE_{eh} \quad (2)$$

where N_{w_i} is the number of electrons in i -th QW layer of device, N_p is the number of photons, ω is the angular frequency, ε_0 is the dielectric constant, Γ_{w_i} is the optical confinement factor for each QW, $v_{g,i}$ is the group velocity, ρ is the density of states, $|\mu|^2$ is the dipole moment, f_c and f_{hh} are the functions of the Fermi distribution for electrons and for heavy holes at thermal equilibrium, respectively, L is the Lorentzian lineshape function and E_{eh} is the transition energy. Photon number at the 3-dB saturation is determined by the following equation:

$$N_{p,s} = \Gamma_w V_w \varepsilon_0 \bar{n}^2 / (\tau_e + \tau_h) \pi L |\mu|^2 \omega, \quad (3)$$

where V_w is the volume of QW layer, n is the refractive index, τ_e and τ_h are the intra-band relaxation times for electrons and holes, respectively. The modal gain is calculated by multiplying the material gain by the optical confinement factor for each QW, which, for the TE mode, can be described by [17]

$$\Gamma_{w_i} = t_{w_i} / \left(t_{tot} + \frac{2}{t_{tot}(\varepsilon_a - \varepsilon_b)} \sqrt{\frac{\varepsilon_b}{\varepsilon_{w_i}}} \left(\frac{\lambda_i}{2\pi} \right)^2 \right) \quad (4)$$

where ε_{w_i} , ε_b and $\varepsilon_a = \frac{1}{t_{tot}} \sum_{w,b} \varepsilon_w t_w + \varepsilon_b t_b$ are the effective permittivity for an active layer, barrier and whole multiple quantum well structure, respectively, t_{tot} is the total thickness of the structure including multiple quantum wells t_a and barriers t_b , and λ_i is the transition wavelength for each QW. The total gain spectrum for the AMQW structure is calculated as a sum of gain spectra for all quantum wells at a constant angular frequency:

$$G_{AMQW}(\omega) = \sum_{i=1}^6 G_i(N_{w_i}, N_p, \omega) \quad (5)$$

Using the fitting formula proposed here, we incorporate the carrier dependent capture efficiency into

SOA model [15] and calculate the optical gain spectra under different pumping current for structure presented in Fig. 1a. The values of main parameters for calculation are presented in [15]. The calculated results are presented in Fig. 4.

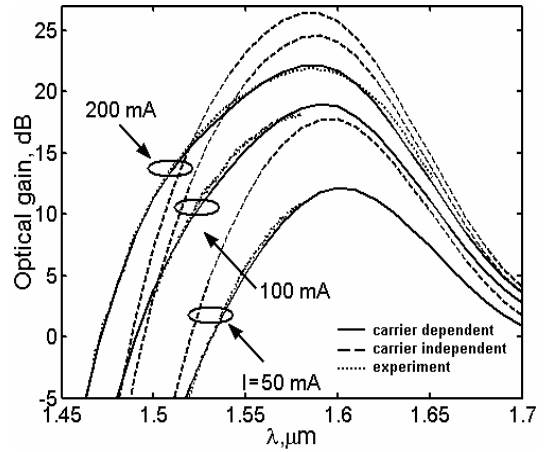


Fig. 4. Experimental and calculated optical gain spectra for different pumping currents.

The gain spectra with concentration-dependent capture efficiency, concentration-independent capture efficiency and experimental data are presented by solid, dashed and dotted lines, respectively. At small pumping currents the optical gain for concentration-independent capture efficiency overestimates the experimental gain value in the whole gain bandwidth. But at large pumping currents there is overestimation on the long wavelengths and underestimation on the short ones. This is because in this case the relation between capture efficiencies for different QWs is constant irrespectively to pumping current. As a result deeper QWs will produce larger gain than shallow ones under any pump current. Account for the concentration dependence of capture efficiency leads to excellent agreement of the theoretical curves and experimental ones. In the range of currents 50-100 mA the capture efficiency droops more rapidly in deeper QWs, as it is shown in inset of Fig. 4. The capture efficiency in shallow QWs also decreases, but more slowly. As a consequence the gain on the long wavelengths will increase more quickly while the rise of the gain on the long wavelengths will slow down under increment of the pumping current. This leads to broadening of the gain spectrum and excellent matching to experimental data.

5. Conclusions

We have developed the model to account for the dependence of the capture efficiency on 2D carrier concentration in the complex AMQW SOA. The carrier-dependent capture efficiency is calculated for SQW structures with different material composition as well as for AMQW structure. We have proposed a fitting formula for concentration dependence of capture efficiency, which

can be easily incorporated into the rate equations providing simple account for inhomogeneous carrier distribution in each active layer of device and its influence on the SOA amplification properties.

Results on the carrier dependence of capture efficiency allows to get the correct value of maximal gain and leads to the enhancement of the optical gain in short-wavelength region at larger pumping currents. With a fixed parameter set, we have achieved the excellent fitting of the experimental measurements for the whole ranges of carrier injection and for a wavelength range of more than 160 nm. Indeed, our findings open up new insights for a more precise simulation of AMQW SOA with an expected impact on device designs.

Acknowledgements

This work is supported by Korean Ministry of Science and Technology through the National Program for Tera-Level Nano Devices "Convocatoria Institucional de Apoyo a la InvestigaciÓ N 2005 000008/05", Mexico.

References

- [1] T. Mukai, Y. Yamamoto, *IEEE J. Quantum Electron* **17**, 1028 (1981).
- [2] P. J. A. Thijs, L. F. Tiemeijer, J. J. M. Binsma, T. van Dongen, *IEEE J. Quantum Electron* **30**, 477 (1994).
- [3] A. V. Uskov, T. W. Berg, J. Mørk, *IEEE J. Quantum Electron* **40**, 306 (2004).
- [4] S. Ikeda, A. Shimizu, T. Hara, *Appl. Phys.Lett.* **55**, 1155 (1989).
- [5] X. Zhu, D. Cassidy, M. Hamp, D. Thompson, B. Robinson, Q. Zhao, M. Davies, *IEEE Photon. Technol. Lett.* **9**, 1202 (1997).
- [6] L. Nguyen, A. J. Lowery, P. C. R. Gurney, D. Novak, *IEEE J. Select. Topics Quantum Electron.* **1**, 494 (1995).
- [7] N. Tessler, G. Eisenstein, *IEEE J. Quantum Electron* **6**, 1586 (1993).
- [8] A. Reale, A. D. Carlo, P. Luigli, *IEEE J. Select. Topics Quantum Electron.* **7**, 293 (2001).
- [9] S. Ikeda, A. Shimizu, *Appl. Phys. Lett.* **61**, 1016 (1992).
- [10] S. M. Sze, *Physics of semiconductor devices*, 2nd edition (John Willey & Sons, 1981).
- [11] H. Furukawa, H. Takakura, K. Kuroda, *IEEE Trans. Instr. and Meas.* **50**, 801 (2001).
- [12] T. Katayama, H. Kawaguchi, *Optical Amplifiers and their applications*, OSA TOPS, 150, (2002), edited by Jon Nagel, Shu Namiki, Leo Spiekman OSA, (2002).
- [13] T. Katayama, H. Kawaguchi, *IEEE Photon. Technol. Lett.* **16**, 855 (2004).
- [14] A. Mecozzi, J. Mørk, *IEEE J. Select. Topics Quantum Electron.* **3**, 1190 (1997).
- [15] V. V. Lysak, H. Kawaguchi, I. O. Sukhoivanov, T. Katayama, O. V. Shulika, *IEEE J. Quantum Electron.* **41**, 797 (2005).
- [16] N. Ogasawara, R. Ito, *Jpn. J. Appl. Phys.* **27**, 615 (1988).
- [17] V. K. Kononenko, I. S. Zakharova, Preprint / ICTP.- Trieste, IC/91/63.- 26p. 1991.

*Corresponding author: Lysak@gist.ac.kr